

# Covert connection of filaments

B. Filippov \*

*Pushkov Institute of Terrestrial Magnetism, Ionosphere and Radio Wave Propagation of the Russian Academy of Sciences (IZMIRAN), Troitsk, Moscow 142190, Russia*

Accepted 0000 December 15. Received 0000 December 14; in original form 0000 October 11

## ABSTRACT

We analyse the relationship between two near filaments, which do not show any connection in  $H\alpha$  images but reveal close magnetic connectivity during filament activations in Extreme Ultraviolet (EUV) observations. A twisted flux rope, which connects a half of one filament with another filament, becomes visible during several activations but seems to exist all the time of the filaments presence on the disc. *Solar Dynamic Observatory (SDO)* and *Solar Terrestrial Relations Observatory (STEREO)* observed the region with the filaments from two points of view separated by the angle of about  $120^\circ$ . On 2012 July 27, *SDO* observed the filament activation on disc, while for the *STEREO B* position the filaments were visible at the limb. Nearly identical interaction episode was observed on 2012 August 04 by *STEREO A* on disc and by *SDO* at the limb. This good opportunity allows us to disentangle the 3-D shape of the connecting flux rope and in particular to determine with high reliability the helicity sign of the flux rope, which looks ambiguous in preliminary inspections of on-disc EUV images only. The complex magnetic structure of the region consists of three braided flux ropes in the vicinity of the coronal null point. Using observations of the flux rope fine structure and plasma motions within it from two points of view, we determine the negative sign of helicity of the flux rope, which corresponds to dextral chirality of the filaments. The observations, despite the tangled fine structure in some EUV images, support flux rope filament models. They give more evidence for the one-to-one relationship between the filament chirality and the flux rope helicity.

**Key words:** Sun: activity – Sun: filaments, prominences – Sun: magnetic fields.

## 1 INTRODUCTION

Solar filaments, or prominences as they are called when observed above the limb, are cool plasma formations supported against the gravity by magnetic field high in the corona. Two magnetic configurations are most often considered as a magnetic skeleton of filaments. They are a twisted magnetic flux rope (Rust & Kumar 1994; Low 1996; Lites 2005; Zhang & Low 2005) and a sheared arcade (Pneuman 1983; van Ballegoijen & Martens 1989; Antiochos et al. 1994; DeVore & Antiochos 2000; Martens & Zwaan 2001; Aulanier et al. 2002; Karpen et al. 2003; Mackay, & van Ballegoijen 2005). Both of them have some observational bases and both meet with certain difficulties. Flux ropes become most evident during filament activations and eruptions. However, some authors raise objections against existence of helical structures within filaments before eruptions. They suggest that twisted flux ropes are forming during the eruptions after field line reconnection (Gosling et al. 1995; Antiochos 1998;

Martin 1998b). One of the vague points is how flux ropes appear in the corona. Do they emerge from the convection zone being formed there by convection and differential rotation (Okamoto et al. 2008), or they are created in the corona from potential fields due to photospheric footpoint motions and reconnection (McKenzie & Canfield 2008; Liu et al. 2010; Green et al. 2011) ?

Recently, many observations of flux ropes in the corona were reported (Raouafi 2009; Cheng et al. 2011, 2012; Zhang et al. 2012; Li & Zhang 2013a,b,c; Patsourakos et al. 2013). Low optical thickness of coronal structures in Extreme Ultraviolet (EUV) makes it not so easy to derive the true helicity sign of observed helical structures. In many cases, it is difficult to decide which features are closer to an observer and which are farther. With flux ropes, we cannot be sure which threads are on the upper side of them and which threads belong to the bottom side. A wrong choice leads to the wrong estimation of the helicity sign. Simultaneous observations from different points of view provided by *Solar Dynamic Observatory (SDO)*, and *Solar Terrestrial*

\* E-mail: bfilip@izmiran.ru

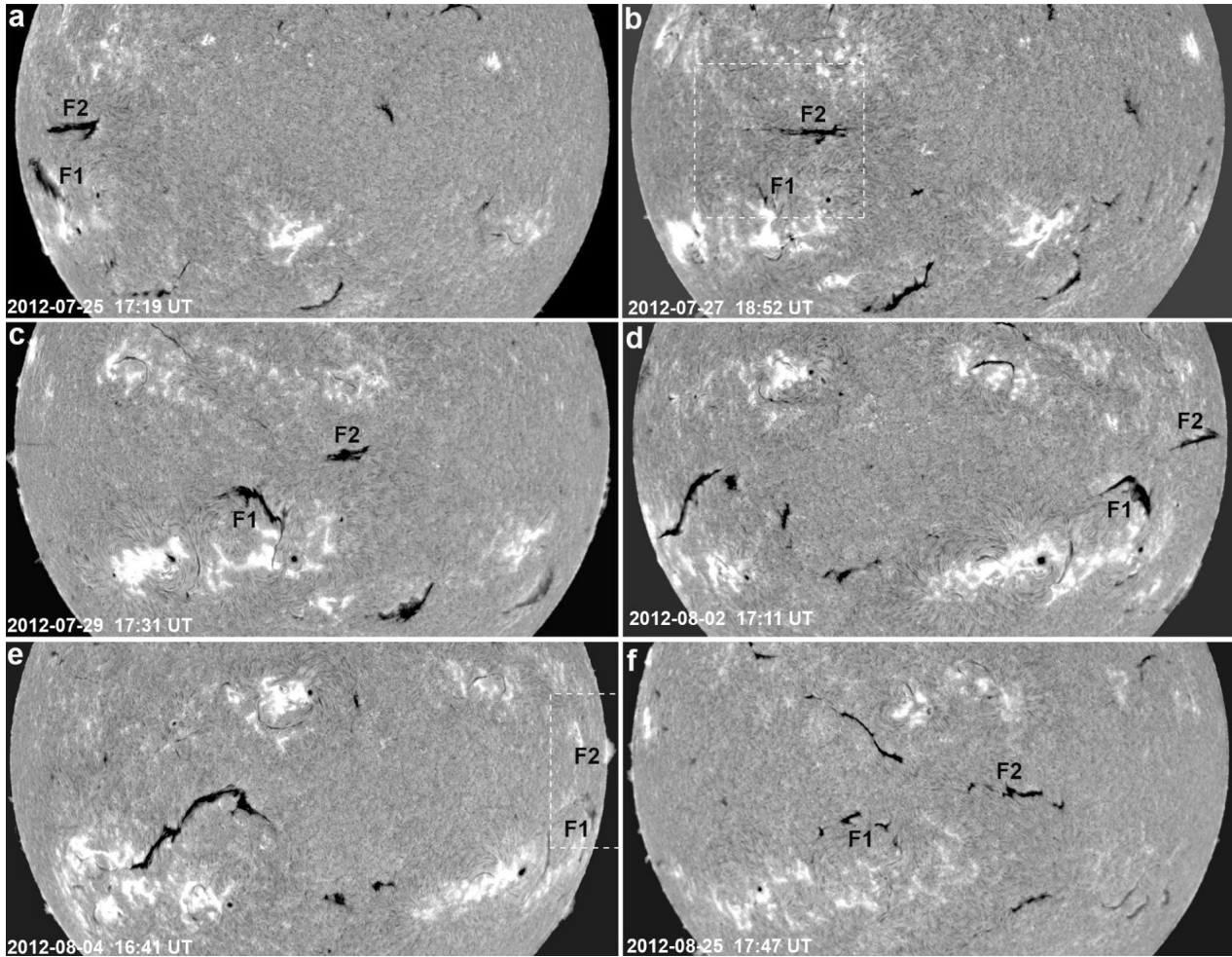


**Figure 1.**  $H\alpha$  filtergrams showing the filaments F1 and F2 during their passage through the solar disc and on the next rotation. White dashed squares correspond to the field-of-view of the images in Fig. 2 and 4. (Courtesy of the Big Bear Solar Observatory).

*Relations Observatory (STEREO)* give good opportunity to reconstruct the 3-D shape of coronal flux ropes.

In active regions, filaments consist of long thin threads stretched along polarity inversion lines (PIL). This hints on the presence of a strong axial magnetic-field component. Indeed, measurements of the magnetic field in prominences showed that the magnetic field in prominences is mostly horizontal and makes an acute angle of about  $20 - 40^\circ$  with respect to the long axis of the prominence (Leroy 1989; Collados et al. 2003; Casini et al. 2003). According to the direction of the axial component of the filament magnetic field relative the surrounding photospheric fields, all filaments can be divided into two classes. A filament is called 'dextral' if the axial component is directed toward the right when the filament is viewed from the side of the positive photospheric polarity, and 'sinistral' if the direction of the axial component is opposite to this (Martin et al. 1994). Usually on both sides of a filament, filament barbs are observed protruding at an acute angle from the main body of the filament. They can be classified as either right-bearing or left-bearing depending on the deviation of the barbs from the axis. In most cases, the barbs of a dextral/sinistral filament are observed to be right/left bearing (Martin 1998a). Thin threads composing the main filament body are deviated at an acute angle clock-

wise to the axis in dextral and counterclockwise in sinistral filaments. This makes it possible to determine the class of a filament (the filament chirality) from its visual appearance, without information on the magnetic fields (Pevtsov et al. 2003).

The bottom parts of helical flux tubes serve as potential wells or magnetic traps where dense and cold plasma can be collected forming the fine structure of the filaments observed in chromospheric lines. During a filament activation or eruption, plasma that moves along field lines can spill over the upper parts of the flux tubes and show both the bottom and upper parts of helices. Recent observations strongly support the idea that dextral filaments are associated with left-handed flux ropes with negative helicity, while sinistral filaments are associated with right-handed flux ropes with positive helicity (Rust 1999; Chae 2000; Joshi et al. 2014).

It was well known for a long time that solar filaments follow large scale PILs of the photospheric magnetic field (Babcock & Babcock 1955; Howard & Harvey 1964; Smith & Ramsey 1967; McIntosh 1972; Snodgrass et al. 2000; Durrant 2002; Ipson et al. 2005). If two PILs are located not far from each other, they can approach closer due to evolution of the photospheric field and change connectivity ('reconnect') after their contact at some point. A pair of filaments

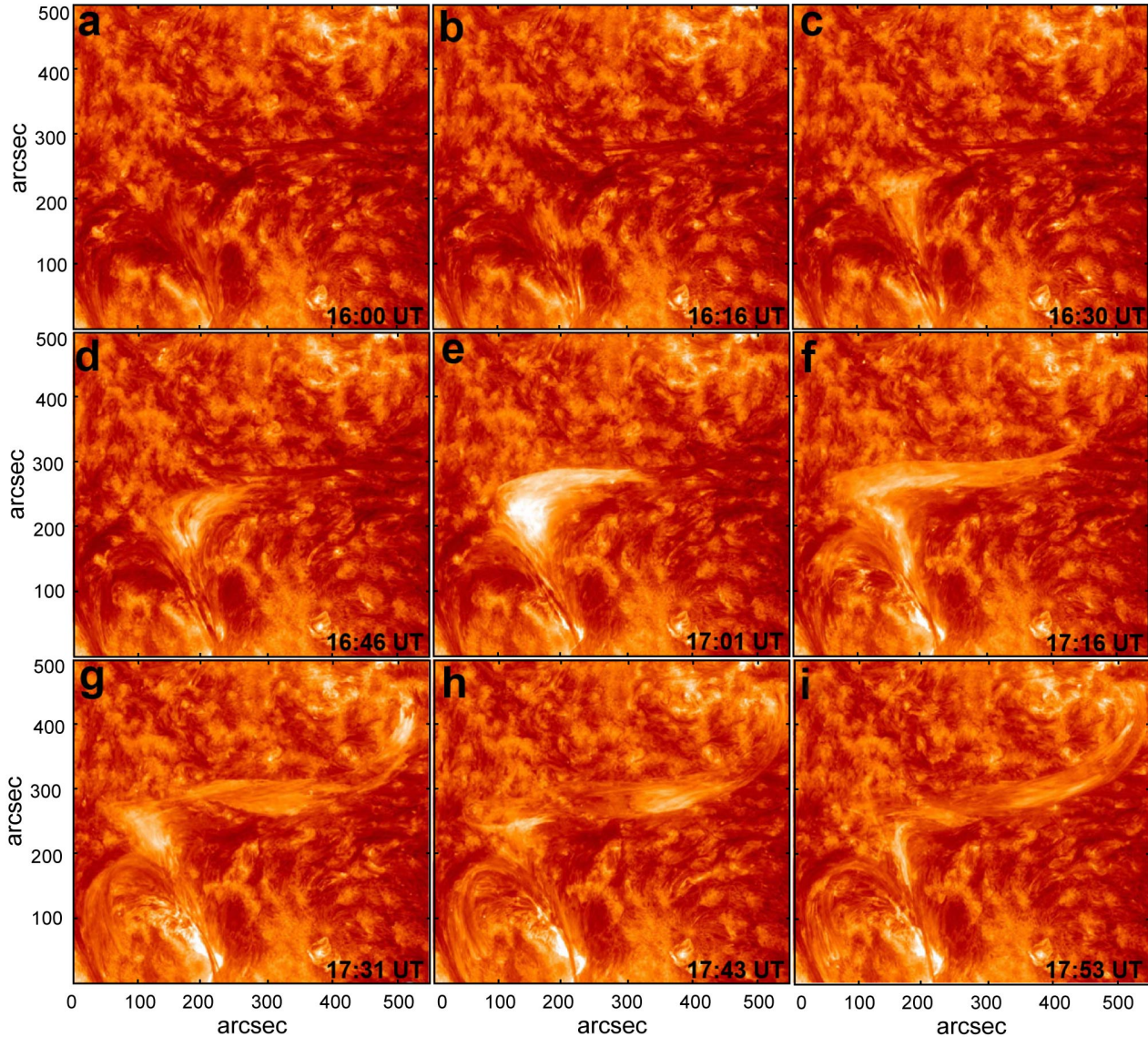


**Figure 2.** Filament activation observed on 2012 July 27 by *SDO*/AIA in the 304-Å channel on disc. (Courtesy of the NASA/*SDO* and the AIA science team.)

of the same chirality may exchange by their halves and also reconnect, while a pair of filaments of the opposite chirality breaks into four independent filaments (Kumar et al. 2010; Chandra et al. 2011; Török et al. 2011; Filippov 2011; Filippov & Srivastava 2011; Filippov 2013a). When two long filaments cross each other to form a cruciform structure, two intersecting PILs correspond to a quadrupole magnetic configuration. There is a null point near the site of intersection in the magnetic field created by photospheric sources.

Merging of short filament segments of the same chirality aligned along the same PIL into a single structure was studied by Schmieder et al. (2004). Two filaments of opposite chirality in the same decaying active region interacted without merging but produced a confined flare (Deng et al. 2002).

In this paper, we analyze the relationship between two near filaments, which do not show any connection in  $H\alpha$  images but reveal the close magnetic connectivity during

filament activations in EUV channels. A twisted flux rope, which connects a half of one filament with another filament, becomes visible during several activations but seems to exist all the time of the filaments presence on the disc. Using observations of the flux rope structure and plasma motions within it from two points of view, we determine the negative sign of helicity of the flux rope, which corresponds to dextral chirality of the filaments.

## 2 DATA AND GENERAL DESCRIPTION OF EVENTS

We used observations of the Big Bear Solar Observatory, *STEREO*, and *SDO*. Synoptic full-disk  $H\alpha$  images (Fig.1) in the end of July and in the beginning of August 2012 show two filaments located not far from each other at a middle latitude in the southern hemisphere. They are marked as F1 and F2 in Fig. 1. The filaments are well developed and



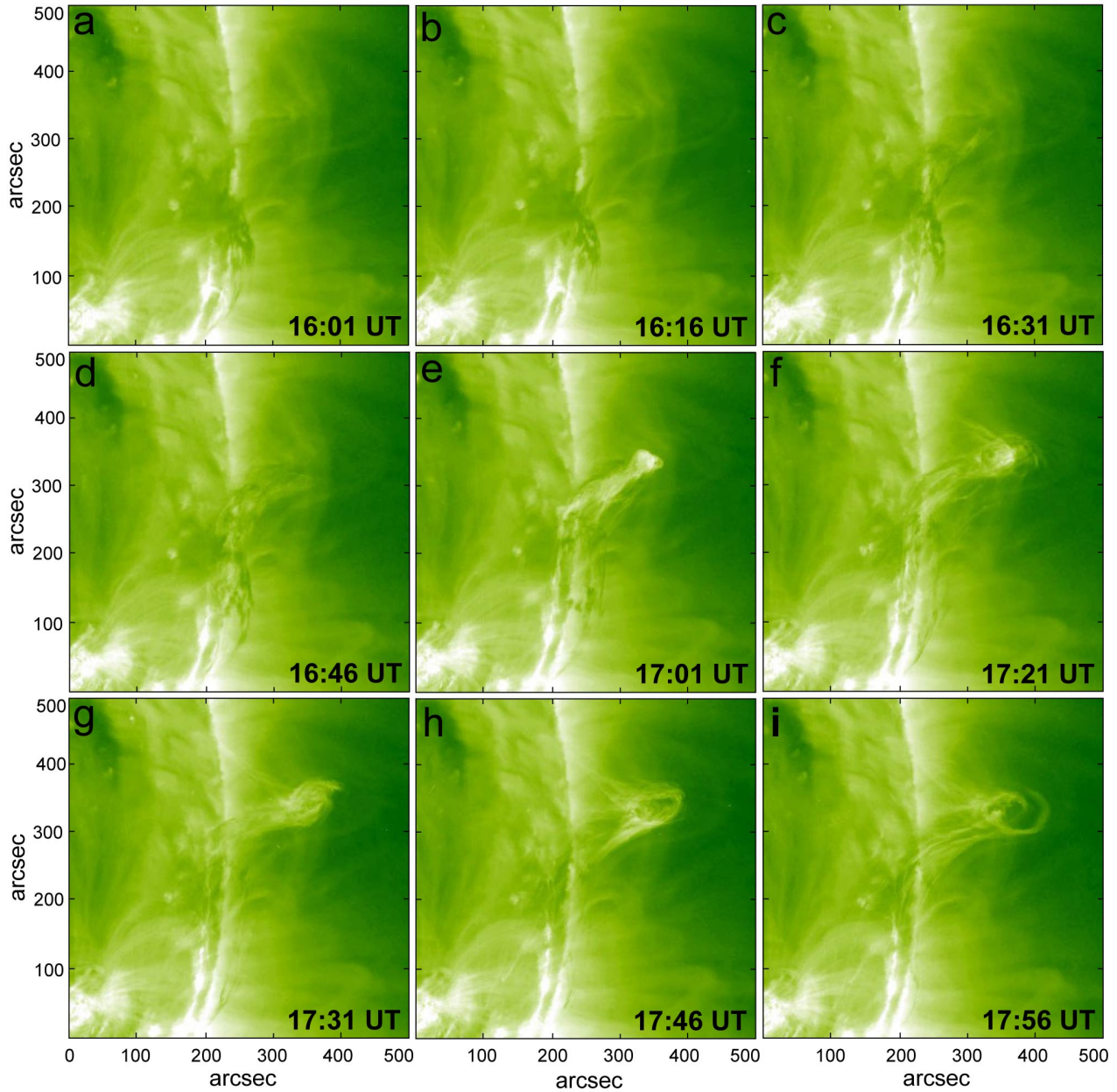


**Figure 3.** Filament activation observed on 2012 July 27 by *STEREO B*/SECCHI in the 195-Å channel at the limb. (Courtesy of the *STEREO*/SECCHI Consortium.)

quite stable. They do not change significantly their shapes during the passage through the solar disc in the end of July and in the beginning of August and can be easily identified on the next solar rotation in the end of August. The filaments seem to be not connected with each other in images in  $H\alpha$  line. However, observations in EUV with the Sun Earth Connection Coronal and Heliospheric Investigation (SECCHI) Extreme Ultraviolet Imager (EUVI; Wuelser et al. 2004; Howard et al. 2008) on board *STEREO* and with the Atmospheric Imaging Assembly (AIA; Lemen et al. 2012) on board the *SDO* (Figs. 2 - 5) show that during activations the filaments reveal the connectivity of their magnetic structures.

Several pulses of filament activations were observed be-

tween July 27 and August 04. The most dramatic events happened on July 27 between 16 and 18 UT, on July 29 between 00:30 and 02:30 UT, and on August 04 between 07 and 10 UT. Each of them starts from brightening at the south-western end of the horseshoe-shaped filament F1. Bright threads elongate along the filament axis showing field aligned motion of hotter plasma. Figs. 2, 3 show the third activation on July 27 observed by *SDO*/AIA in the 304-Å channel on disc and by *STEREO B*/SECCHI in the 195-Å channel at the limb. The separation angle of the *STEREO* spacecraft with the Earth was about  $120^\circ$  in summer 2012. Long thin threads reveal the axial magnetic field in the filament channel. However, most of threads not follow the horseshoe-curved axis of the filament F1 but make nearly

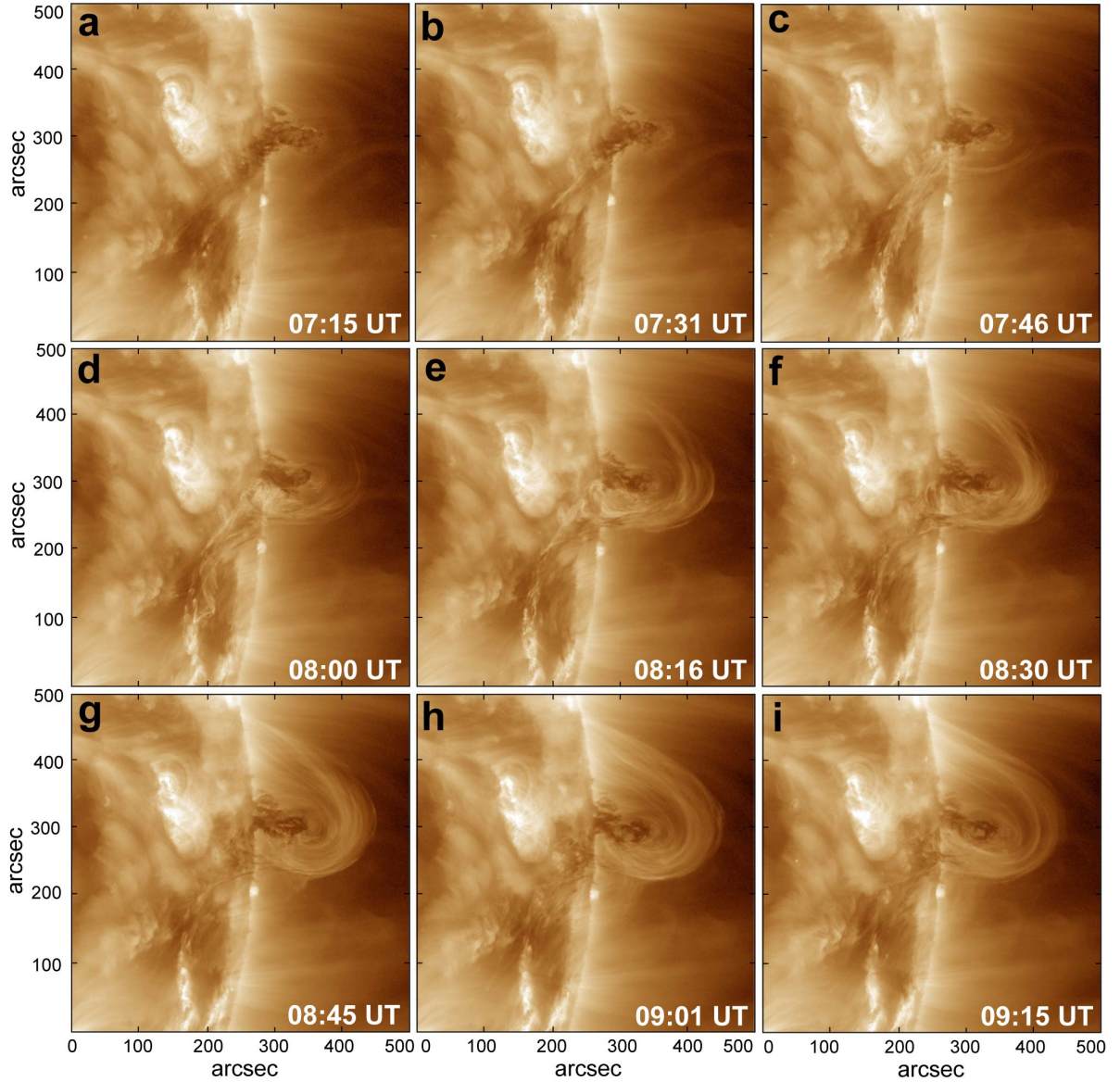


**Figure 4.** Filament activation observed on 2012 August 04 by *SDO*/AIA in the 193-Å channel at the limb. (Courtesy of the NASA/*SDO* and the AIA science team.)

right-angle turn to the west and follow the axis of the filament F2. The eastern part of the filament F1 becomes invisible in  $H\alpha$  images during activations (Fig. 1(b)).

Just the same scenario was observed on 04 August, only the aspect angles for the spacecrafts changed to opposite. *SDO* observed the filaments close to the limb, while *STEREO A* observed events on disc (Figs. 4, 5). Better time and spatial resolution of *SDO*/AIA images allow recognizing finer details in the structure of the filaments both on disc on July 27 and at the limb on August 04. Since the events on both days are very similar, we can expect that the magnetic structure of the filaments has not changed in this period of time and may consider all images as different views of the same structure. Thus, the filaments that look separate and independent in  $H\alpha$  images are contained within a united magnetic structure.

Despite the location in the southern hemisphere, the

chirality of the filament F1 is dextral. This is very evident from the fine structure of the filament in  $H\alpha$  line (Figs. 1 (a), (c), (d), 6). Thin threads within the filament body deviate clockwise from the filament axis (Fig. 6) and filament barbs are right bearing, which both correspond to the dextral chirality. According to one-to-one correspondence between the filament chirality and the enveloping flux rope helicity (Rust & Kumar 1994; Rust 1999; Chae 2000; Pevtsov et al. 2003; Mackay et al. 2010; Chandra et al. 2010; Joshi et al. 2014) we may expect the manifestation of a left-handed flux rope during filament activations. However some images look puzzling.



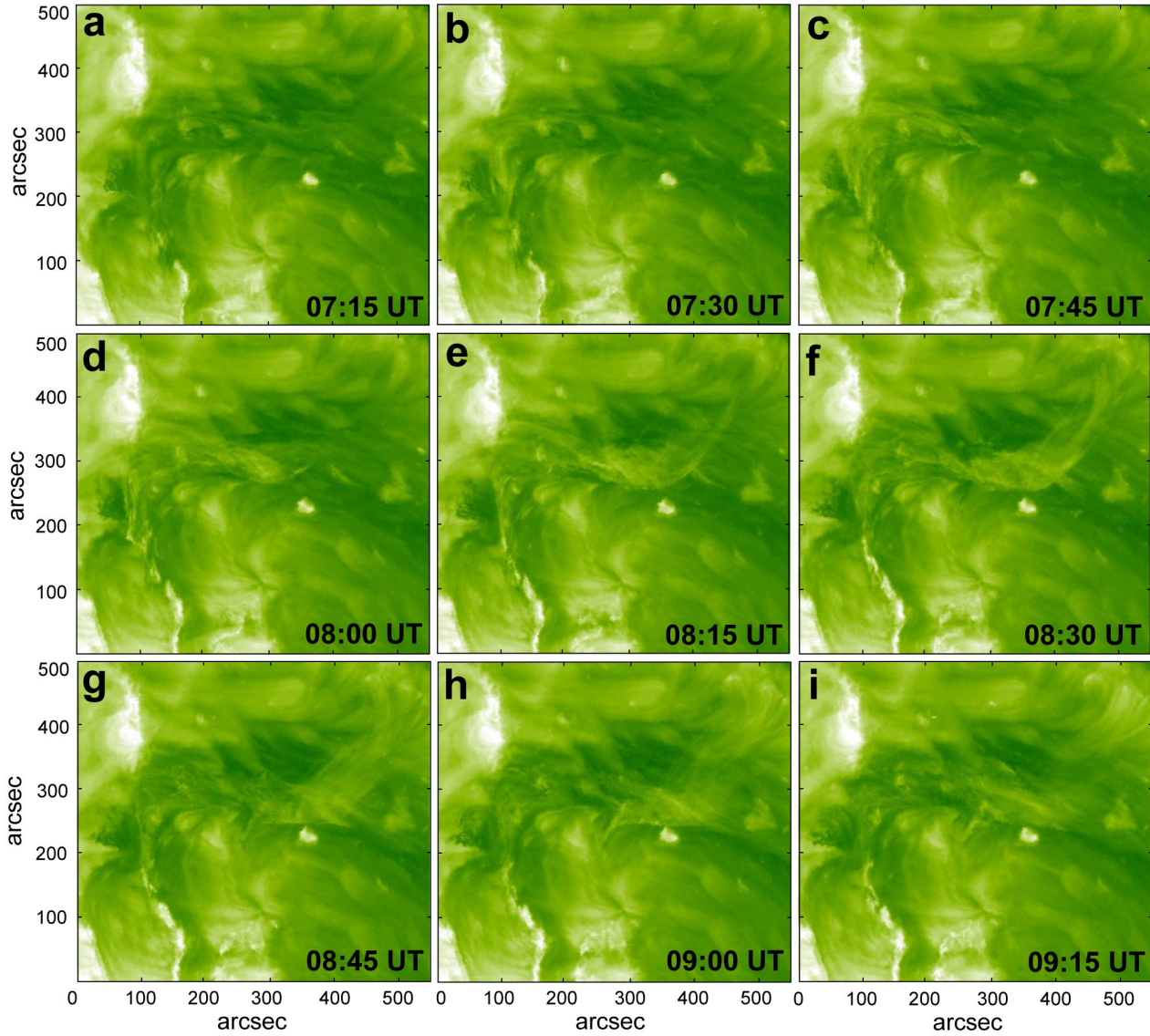


**Figure 5.** Filament activation observed on 2012 August 04 by *STEREO A*/SECCHI in the 195-Å channel on disc. (Courtesy of the *STEREO*/SECCHI Consortium.)

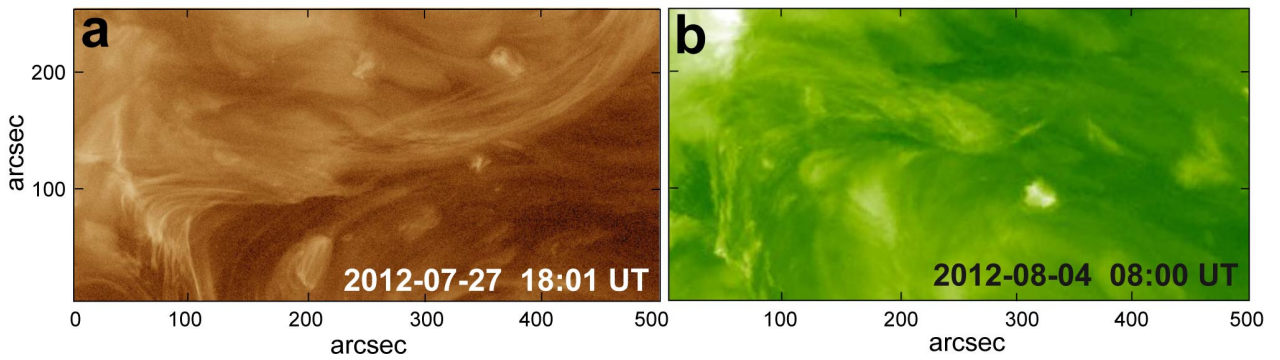


**Figure 7.** Flux-rope structure looking like a right-hand helix observed on 2012 July 27 by *SDO*/AIA in the 193-Å channel (a) and on 2012 August 04 by *STEREO A*/SECCHI in the 195-Å channel (b). (Courtesy of the NASA/*SDO* and the AIA science team and *STEREO*/SECCHI Consortium.)

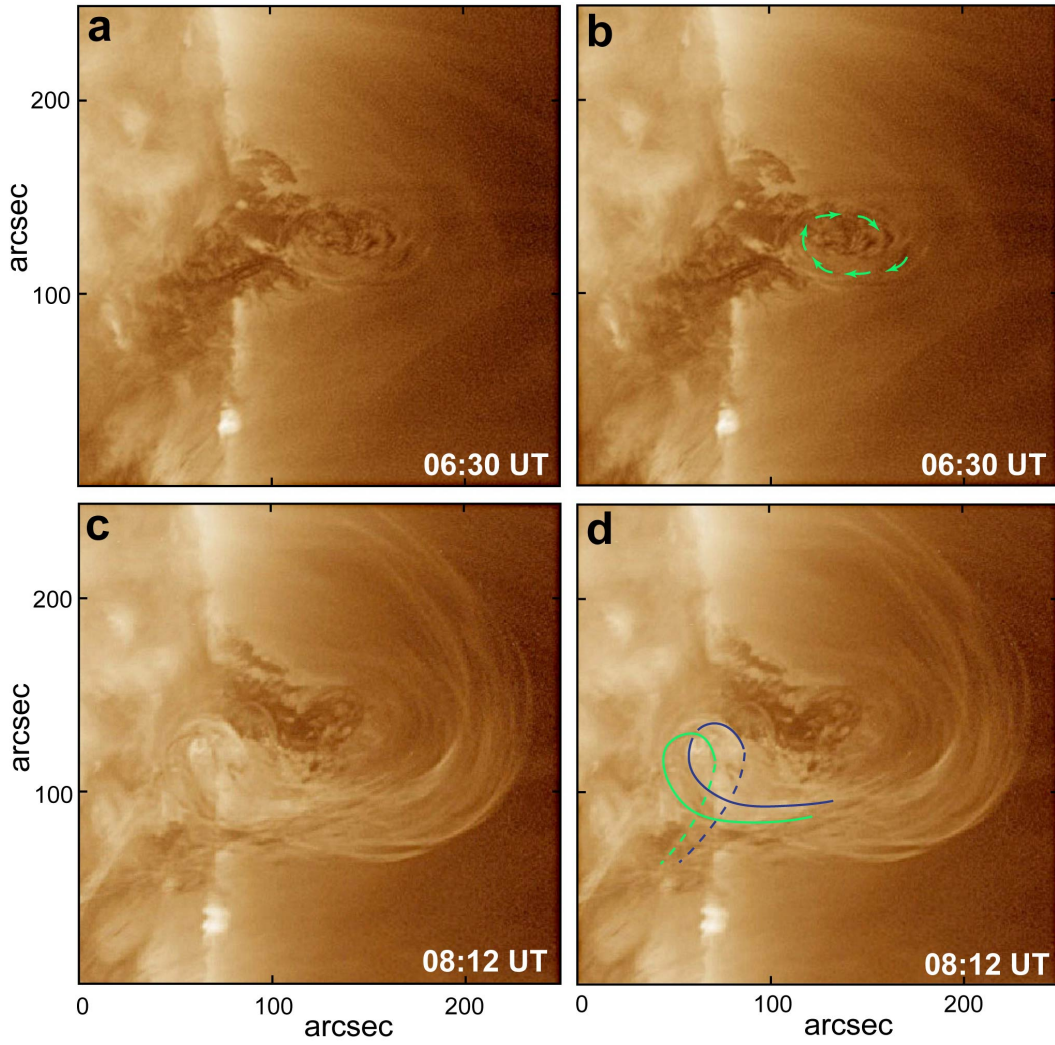


**Figure 8.** Clockwise rotation of elongated blobs within the body of the filament F2 (a), (b) and a loop-like structure at the lower part of the flux rope (c), (d) observed by *SDO/AIA* in the 193-Å channel. (Courtesy of the NASA/*SDO* and the AIA science team.)

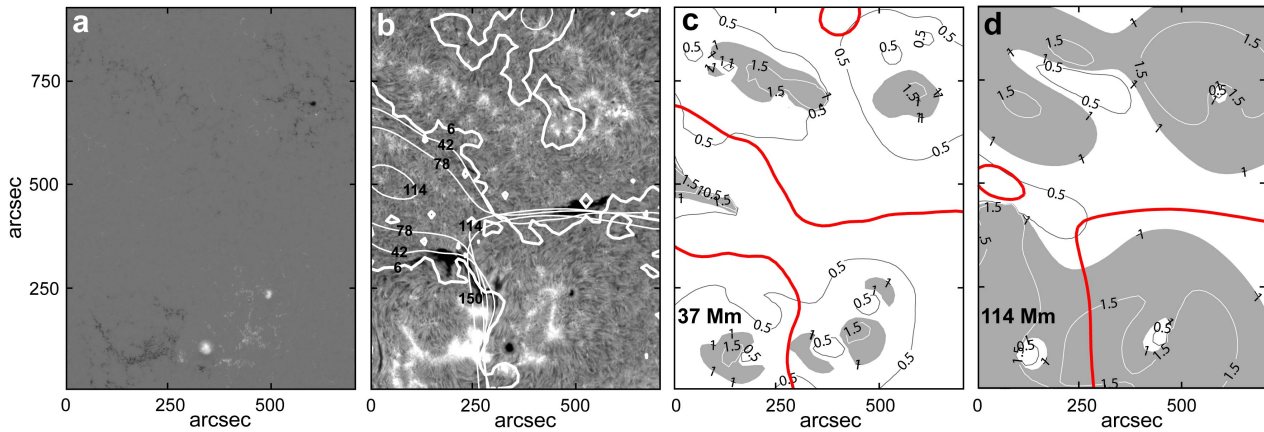


**Figure 10.** Smaller fragment of the HMI magnetogram taken on 2012 July 29 at 17:31 UT (a),  $H\alpha$  filtergram of the same region and at the same time with superposed PILs (b), and distributions of the decay index and PILs (thick red lines) at different heights (c) - (d). Shadowed areas show the regions where  $n > 1$ . (Courtesy of the NASA/*SDO* and the HMI science team and of the Big Bear Solar Observatory.)



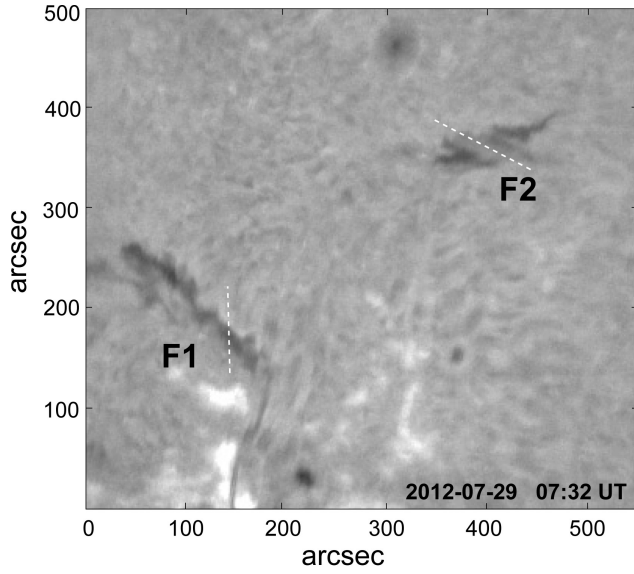


**Figure 6.**  $H\alpha$  spectroheliogram showing the chirality of the filaments F1 and F2. White dashed lines show the direction of filament threads deviating at an acute angle clockwise to the axes of filaments (Courtesy of the Observatory Paris-Meudon).

### 3 PUZZLING STRUCTURES

Beside the covert connection of the filaments F1 and F2 revealed during several activations, some EUV images look puzzling if we keep in mind the expected correspondence between the filament dextral chirality and the negative helicity of the enveloping flux rope. Fig. 7 shows the flux-rope structure looking like a right-hand helix on 2012 July 27 in the *SDO*/AIA image in the 193-Å channel and on 2012 August 04 in the *STEREO A*/SECCHI image in the 195-Å channel (see also Fig. 2(i) and Fig. 5(c) - (e)). Most of thin bright threads forming the flux rope deviate clockwise from the flux-rope axis and only few faint threads are visible deviating counterclockwise. It is unknown for certain which threads are higher and which threads are lower but one can expect that the higher threads would be more noticeable in images. Thus, the structures in Fig. 7 give us impression of a right-hand helix.

Another puzzling feature is a clockwise rotation of elongated blobs within the filament F2 observed by *SDO*/AIA at the limb between 06:15 UT and 07:30 UT (Fig. 8(a), (b), movie.SDO\_04). If activation starts at the south-western end of the filament F1 and propagates from the east to the west along the filament F2, we could expect a counterclockwise rotation of blobs moving along a left-handed helix away from us. Instead, the rotation is clockwise during more than an hour.

One more puzzle is a loop-like structure at the lower part of the flux rope (Fig. 8(c), (d)). The ascending branch of the loop seems to be located in front of other threads. Its continuation runs above the dark body of the filament F2 to the north-west (Fig. 5(d) - (g)). The other ends of the loop-like threads represented by dashed lines in Fig. 8(d) should pass below the ascending branch to the location of the filament F1. Therefore, the most curved segments of the lines correspond to a  $180^\circ$  turn of the threads and show a

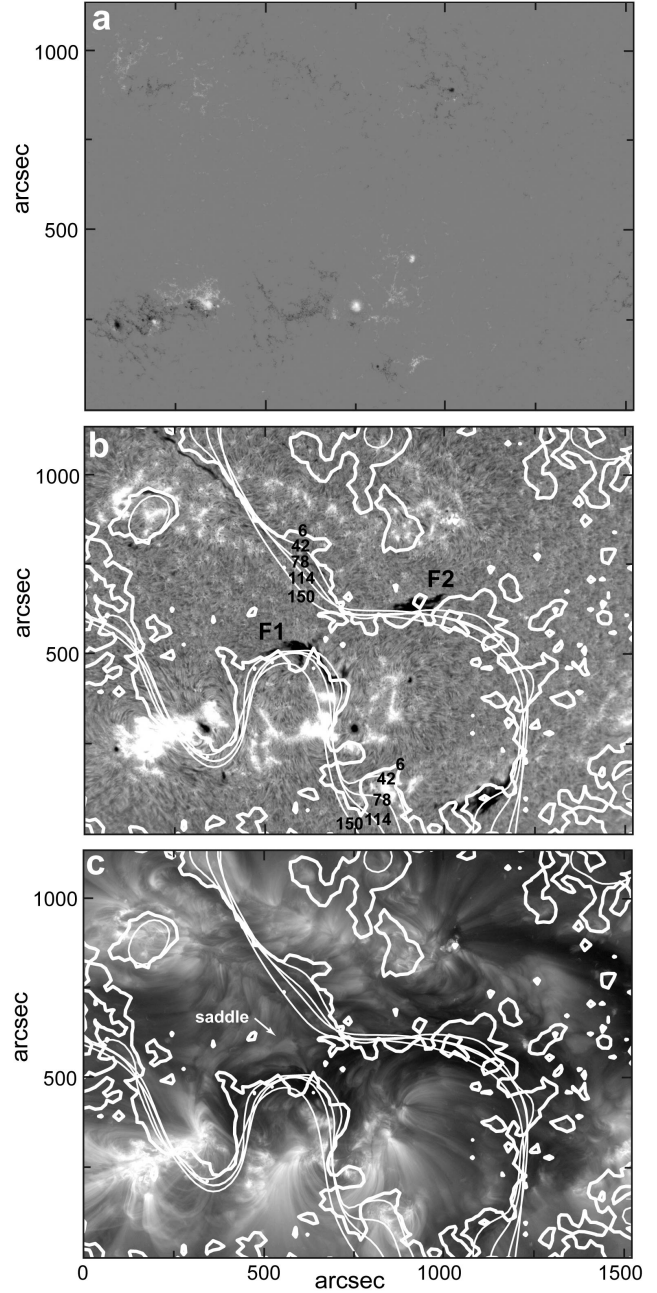


**Figure 9.** Fragment of the HMI magnetogram taken on 2012 July 29 at 17:31 UT containing all most important magnetic sources on the disc (a),  $H\alpha$  filtergram of the same region and at the same time with superposed PILs at a height of 6 (thick lines), 42, 78, 114, and 150 Mm (b), *SDO*/AIA image in the 193-Å channel with superposed PILs (c). (Courtesy of the NASA/*SDO* HMI and AIA science teams and of the Big Bear Solar Observatory.)

real loop. There is no evidence of such a loop in *STEREO A*/SECCHI images in a view from above (Fig. 5).

In order to recognize the true geometry of the observed structures we need more detailed and careful examination of all images and correlation of them with a presumable magnetic configuration.



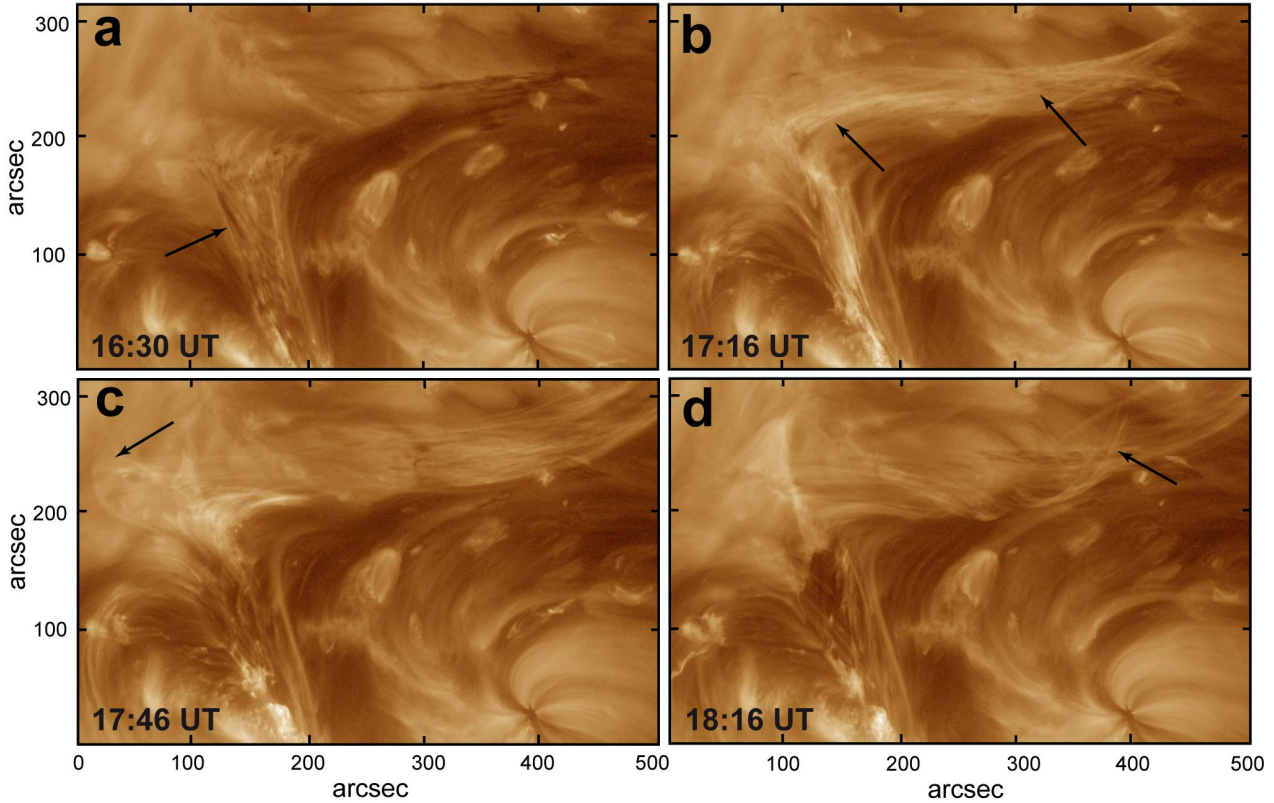


**Figure 11.** Filament structure observed on 2012 July 27 by *SDO/AIA* in the 193-Å channel, which show features undoubtedly corresponded to left-hand helix (a), (b), (d) and very curved threads above the saddle (c). (Courtesy of the NASA/*SDO* and the AIA science team.)

#### 4 MAGNETIC CONFIGURATION

When two long filaments cross each other to form a cruciform structure, two intersecting PILs correspond to a quadrupole magnetic configuration. Our filaments F1 and F2 do not approach very close to each other and do not demonstrate any connection in a quiescent state. However every activation reveals the field lines that connect them.

##### 4.1 Polarity Inversion Lines of Potential Magnetic Field

Fig. 9(a) shows a fragment of the magnetogram taken by the Heliospheric and Magnetic Imager (HMI; Schou et al. 2012) on board *SDO* on 2012 July 29 at 17:31 UT when the filaments F1 and F2 were close to the central meridian (Fig. 1(c)). The fragment contains all most important magnetic sources on the disc. Using this magnetogram as the boundary condition for the potential magnetic field calculations we calculate  $B_z$  maps ( $z$ -axis is vertical) at different heights and obtain a set of PILs  $B_z = 0$ . We solve the Neuman external boundary value problem numerically using the Green function method (Filippov & Den 2000, 2001; Filippov 2013b). Our numerical code of a potential field extrapolation is more suitable for rather small solar areas because it assumes the considered photospheric area as a flat surface. The fragment in Fig. 9(a) covers a large part of the disc and does not fit to this condition. Therefore we will consider the results of calculations as a rough approximation.

In Figs. 9(b), (c) the PILs are superposed on the  $H\alpha$  filtergram and on the 193-Å filtergram. The lowest PIL at a height of 6 Mm is shown by a thicker line. The higher PILs do not approach closer as it sometimes happens in quadrupolar configurations (Filippov & Srivastava 2011; Filippov 2011). However a saddle-like structure is visible near the closest approach of the PILs (Fig. 9(d)). It manifests the real presence of the quadrupolar configuration.

If we cut a smaller fragment from the same HMI magnetogram (Fig. 10(a)), the result is different. At the height of about 100 Mm, PILs running above the filament F1 turn to the west and run above the filament F2 (Fig. 10(b)). At these heights, a flux rope can exist, which is able to contain both the south-western part of the filament F1 and the filament F2. The flux rope is in horizontal equilibrium on the PIL. Stable vertical equilibrium is possible only if the so-called decay index  $n = -d \ln B / d \ln h$  of the surrounding magnetic field is less than the critical value  $n_c$  (van Tend & Kuperus 1978; Bateman 1978; Forbes & Isenberg 1991; Lin et al. 1998; Kliem & Török 2006; Fan & Gibson 2007; Isenberg & Forbes 2007; Démoulin & Aulanier 2010; Olmedo & Zhang 2010; Nindos et al. 2012). The exact value of  $n_c$  depends on parameters of a flux-rope model and varies between 1 and 1.5 (van Tend & Kuperus 1978; Bateman 1978; Filippov & Den 2000, 2001; Démoulin & Aulanier 2010). Figs. 10(c)-(d) show the distribution of the decay index at heights of 37 and 114 Mm. At the height of 37 Mm, the shadowed area  $n > 1$  first touches the PIL near the south-western end of the filament F1. Possibly, it is connected with the initiation

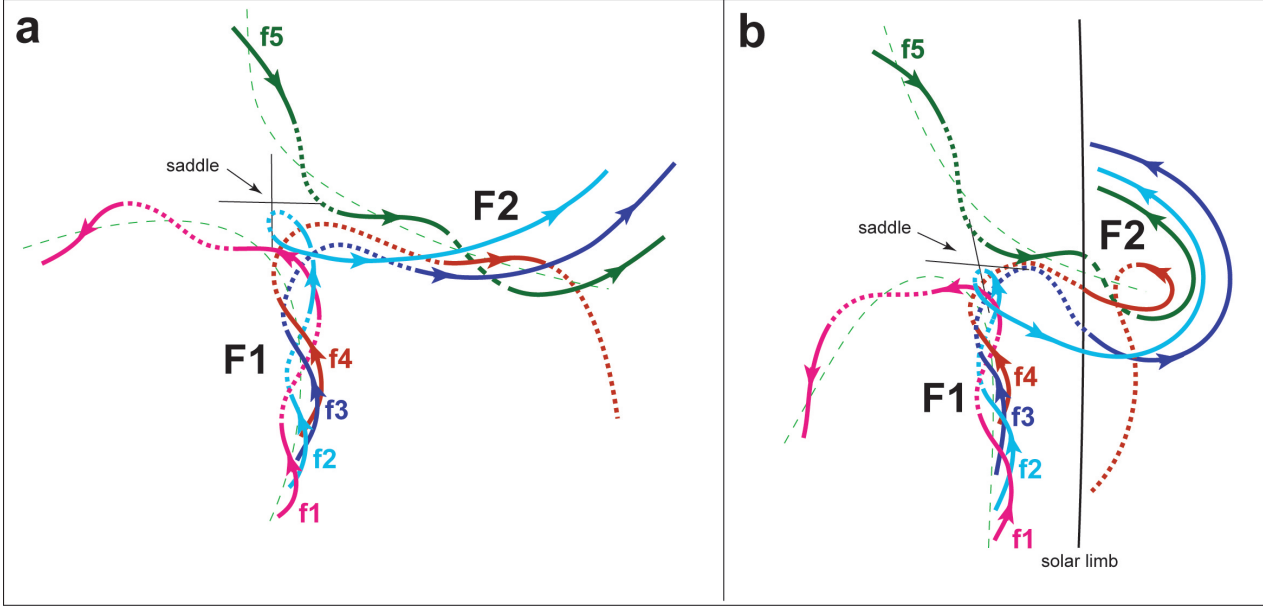


**Figure 12.** Scheme of the magnetic field structure of two filaments. Top view (a) and side view (b).

of all activations in this place. The area around the filament F2 is stable up to the heights much above 100 Mm.

The results shown in Fig. 10 are also a rough approximation. On the one hand, the boundary area is smaller and closer to the flat surface. On the other hand, some strong magnetic sources are not taken into account. Particularly, these are active regions to the east from the selected area. They 'attract' the PIL and do not allow it to turn to the west in Fig. 9 like it does at high heights in Fig. 10. Despite of their roughness, the results of potential magnetic field calculations confirm the presence of the quadrupolar magnetic configuration at the place where the filaments approach each other and show the possibility of the existence of the stable flux rope connecting the filaments F1 and F2.

#### 4.2 Fine Structure of the Flux Rope

It is most probable that flux tubes connecting the vicinities of F1 and F2 exist at all times during their passage through the solar disc in the end of July and in the beginning of August. They become visible after F1 activations when they are filled with both hot and cold plasmas. Evidently they are twisted into a flux rope. This flux rope can consist of some strands of the flux ropes containing the main bodies of the filaments F1 and F2 or be a separate flux rope like in double-decker filaments (Liu et al. 2012; Kliem et al. 2014).

Coronal images give us 2-D projections of real 3-D coronal structures. Sometimes, it is difficult to derive the true geometrical shape of observed formations from only one projection. In a case of flux ropes, it may lead to estimation of wrong sign of helicity if we do not know whether observed features belong to the frontal or far side of the flux rope. Observations from another view point and internal motions within the formation allow us to derive more correctly the 3-D geometry of it.

Observations at the western limb (Figs. 3, 4, movie\_STB\_27, movie\_SDO\_04) show bright plasma moving

from the south to the north along high loops above the body of the filament F2. The height of the top of the loops is about 140 Mm and the height of the prominence top is about 70 Mm. Since on-disc observations (Figs. 2, 5, movie\_SDO\_27, movie\_STA\_04) show at the same time plasma propagating along the inverted-'S'-shaped axis of the interconnecting flux rope from its south-eastern end to the north-western end, the motion corresponds to a field-aligned motion within a left-hand helix. After each plasma injection into the flux rope at its south-eastern end, some bright and dark features move back demonstrating at times counterstreaming. Such backward motion can be recognized in *STEREO A/SECCHI* images on disc in the 195-Å channel on 2012 August 04 between 06:45 UT and 07:05 UT. The backward motion within a left-hand helix corresponds to the clockwise rotation observed by the *SDO/AIA* at the limb (Fig. 8(a), (b), movie\_SDO\_04).

More detailed examination of a sequence of images shows that the threads deviating clockwise from the filament axis (Fig. 7) are located at the bottom side of the flux rope. There are no clear cases of their overlaying the threads that deviate counterclockwise, while opposite examples can be easily found (Fig. 11). Nevertheless, most convincing arguments proving the left-handedness of the flux rope are in the comparison of plasma motion in two projections. During a 'westward' motion (from the south-western end of the filament F1 to the western end of the filament F2), observations at the limb show a counterclockwise rotation, while a 'eastward' motion corresponds to a clockwise rotation. A nearby sunspot visible at the right-hand bottom corner of Fig. 11 also demonstrates negative helicity. Coronal loops connected to the sunspot compose a pattern of a counterclockwise whirl. Such counterclockwise whirls are more typical for the northern hemisphere but here this is an exception together with the dextral chirality of the filaments. Rust & Martin (1994) found that filaments with an end curving toward sunspots with counterclockwise/clockwise whirls are always dextral/sinistral. Although this sunspot is not con-



nected to filament ends, it shows the dominating helicity of the region.

In addition to the obvious field-aligned motion, the whole system of thin threads moves in the direction to the center of the saddle structure between 16:45 UT and 17:30 UT on July 27, then returns to the previous position on the periphery of the saddle by 17:52 UT, and makes new rush to the center between 16:53 UT and 18:11 UT. The velocity of the field-aligned motion of different features is about  $100 \pm 10 \text{ km s}^{-1}$ . The velocity of the transversal motion of threads during their first rush in the direction to the center of the saddle is  $70 \pm 2 \text{ km s}^{-1}$ . Rapid displacements of entire long threads mean rapid changes of the magnetic field possibly caused by some instability (kink, torus). At the beginning of several activations, a displacement of counterclockwise deviated threads from the left side of the flux rope to the right side is observed (for example, between 14:20 UT and 14:57 UT on July 27, see movie\_SDO\_27). This motion corresponds to untwisting of a left-hand helix and such untwisting is observed in many eruptive events.

Fig. 12 presents a scheme of the magnetic structure of the two filaments under study. We assume that each of the filaments is contained in a left-handed flux rope according to their dextral chirality. Field lines f1 and f5 in Fig. 12 represent these flux ropes. There is also a flux rope represented by field lines f2, f3, and f4 connecting the filaments F1 and F2. This flux rope is located on the PIL turning to the west nearly at a right angle close to the saddle as shown in Fig. 10. The fine structure and internal field-aligned plasma motions show also the negative helicity of the flux rope. It is not loaded with cold dense plasma and not visible as a filament in  $H\alpha$  images. However, it is revealed many times in EUV at the time of filament activations during the passage of the region through the solar disc, which proves its permanent existence. The interconnecting flux rope can be composed by a number of strands of the flux ropes containing the main bodies of the filaments F1 and F2, which split in the vicinity of a null point at the center of the saddle, or be the separate flux rope like in double-decker filaments. The field line f4 represents the threads that propagate to the south of the filament F2 axis around 09 UT on August 04 (Fig. 4(g) - (i), Fig. 5(f) - (i), movie\_SDO\_04). The field line f2 represents the threads making up the loop shown in Fig. 7(c), (d). This line approaches closest to the null point and is most curved, as pointed by the arrow in Fig. 11(c), because of the sharp changes in the field line geometry near the null point.

The scheme in Fig. 12 is derived from the observed fine structure of the interacting filaments. However, it is very similar to the magnetic configuration being formed after two flux ropes reconnection in the MHD simulation of Török et al. (2011). Due to the continuous changes of the boundary conditions in the simulations, the configuration with four braided flux ropes exists only a rather short period of time. In our case, the configuration is not as symmetric as in the simulation. Only one interconnecting flux rope is observed and it exists a long time, possibly, because of the slow changes in the surrounding photospheric magnetic fields.

## 5 SUMMARY AND CONCLUSIONS

Two filaments located not far from each other at a middle latitude in the southern hemisphere look to be separate and independent in  $H\alpha$  images in the end of July and in the beginning of August 2012. The chirality of both filaments is dextral in violation of the general hemispheric rule. The filaments do not change significantly their shapes during the passage through the solar disc. During several pulses of filament activations observed between July 27 and August 04, a flux rope connecting both filaments becomes visible in EUV channels. Numerous appearances and disappearances of the connecting flux rope at the same place and with the same structure in EUV observations show that this magnetic flux rope exists permanently but becomes visible only during activations when it is filled with emitting and absorbing plasma. However, the fine structure of the flux rope in EUV images is rather tangled. At first glance it is difficult to determine even the helicity sign of the flux rope, or handedness of the observed helix, because it is not so easy to decide to what side of the flux rope, frontal or back, visible features belong (Joshi et al. 2014; Filippov et al. 2015). Only the advantage of multi-view-point observations provided by the *SDO* and *STEREO* missions and observations of plasma motions within the flux rope gives the opportunity to determine reliably the true sign (negative) of helicity. This sign of the flux-rope helicity corresponds to the dextral chirality of both filaments.

As is well known, flux ropes are in horizontal equilibrium when they follow PILs of the ambient magnetic field. Each filament, F1 and F2, is embedded into its own flux rope, which follows its own PIL (see Fig. 9). The interconnecting flux rope should also follow a PIL. Therefore, the PIL should exist that connects two filament channels at some height. Such change in PIL connectivity is possible only near a null point. EUV observations really show the presence of a saddle structure at the place of the closest approachment of the filaments. The center of the saddle structure is a two-dimensional X-point. The horizontal field vanishes there owing to the symmetry of the structure. If a PIL, at which the vertical field is zero, crosses the saddle, this means the existence of a 3-D null point.

Our potential magnetic field calculations have very limited accuracy because of the characteristic of the photospheric magnetic field distribution in the region. Choosing a limited photospheric area as the boundary condition, we can obtain PILs connecting the two filament channels (Fig. 10). However, the PIL connectivity depends on the size of the chosen area. Anyway, these calculations show the possibility of the existence of the PIL connecting the two filament channels, which is manifested more exactly by the presence of the stable flux rope.

The filament activation includes the heating of the plasma and field-aligned motions within the filament body and the enveloping flux rope. The velocity of the field-aligned motion of different features is about  $100 \pm 10 \text{ km s}^{-1}$ . At some moments, a section of the whole interconnecting flux rope near the saddle moves towards the null point with a velocity of  $70 \pm 2 \text{ km s}^{-1}$ . Then it returns back. Sometimes, the rotation of the flux-rope threads corresponding to its unwinding is observed.

The considered example of filament interaction demon-

strates the complex magnetic structure of the region, which is not evident in  $H\alpha$  observations. It consists of three braided flux ropes in the vicinity of the coronal null point. The observations, despite the tangled fine structure in some EUV images, support flux rope filament models. They give more evidence for the one-to-one relationship between the filament chirality and the flux rope helicity.

## ACKNOWLEDGMENTS

The author acknowledges the Big Bear Solar Observatory, Observatory Paris-Meudon, *STEREO*, *SDO* teams for the high-quality data supplied. The author thanks the referee for critical comments and useful suggestions. Movies created using the ESA and NASA funded Helioviewer Project. This work was supported in part by the Russian Foundation for Basic Research (grant 14-02-92690).

## REFERENCES

- Antiochos S. K., 1998, *ApJ*, 502, L181  
 Antiochos S. K., Dahlburg R. B., Klimchuk J. A., 1994, *ApJ*, 420, L41  
 Aulanier G., DeVore C. R., Antiochos S. K., 2002, *ApJ*, 567, L97  
 Babcock H. W., Babcock H. D., 1955, *ApJ*, 121, 349  
 Bateman G., 1978, *MHD Instabilities*, Massachusetts Institute of Technology, Cambridge, MA.  
 Casini R., López Ariste A., Tomczyk S., Lites B. W., 2003, *ApJ*, 598, L67  
 Chae J., 2000, *ApJ*, 540, L115  
 Chandra R., Pariat E., Schmieder B., Mandrini C. H., Uddin W., 2010, *Sol. Phys.*, 261, 127  
 Chandra R., Schmieder B., Mandrini C. H., Démoulin P., Török T., Pariat E., Uddin W., 2011, *Sol. Phys.*, 269, 83  
 Cheng X., Zhang J., Liu Y., Ding M. D., 2011, *ApJ*, 732, L25  
 Cheng X., Zhang J., Saar S. H., Ding M. D., 2012, *ApJ*, 761, 62  
 Collados M., Trujillo Bueno J., Asensio Ramos A., 2003, in Trujillo Bueno J., Sánchez Almeida J., eds, *ASP Conf. Ser.* 236, *Solar Polarization Workshop 3*, Astron. Soc. Pacific, San Francisco, p. 468  
 Démoulin P., Aulanier G., 2010, *ApJ*, 718, 1388  
 Deng Y., Lin Y., Schmieder B., Engvold O., 2002, *Sol. Phys.* 209, 153  
 DeVore C. R., Antiochos S. K., 2000, *ApJ*, 539, 954  
 Durrant C. J., 2002, *Sol. Phys.*, 211, 83  
 Fan Y., Gibson S. E., 2007, *ApJ*, 668, 1232  
 Filippov B. P., 2011, *Astron. Rep.*, 55, 541  
 Filippov B., 2013a, in Schmieder B., Malherbe J.-M., Wu S. T., eds, *Proc. IAU Symp. 300, Nature of Prominences and their Role in Space Weather*, Cambridge University Press, Cambridge, UK, p. 412  
 Filippov B., 2013b, *ApJ*, 773, 10  
 Filippov B.P., Den O.G., 2000, *Astron. Lett.*, 26, 322  
 Filippov B.P., Den O.G., 2001, *J. Geophys. Res.*, 106, 25177  
 Filippov B., Srivastava A. K., 2011, *Sol. Phys.*, 270, 151  
 Filippov B., Srivastava A. K., Dwivedi B. N., Masson S., Aulanier G., Joshi N. C., Uddin W., 2015, *MNRAS*, 451, 5636  
 Forbes T.G., Isenberg P.A., 1991, *ApJ*, 373, 294  
 Gosling J. T., Birn J., Hesse M., 1995, *Geophys. Res. Lett.*, 22, 869  
 Green L. M., Kliem B., Wallace A. J., 2011, *A&A*, 526, A2  
 Howard R. F., Harvey J. W., 1964, *ApJ*, 139, 1328  
 Howard R.A. et al., 2008, *Space Sci. Rev.*, 136, 67  
 Ipson S. S., Zharkova V. V., Zharkov S., Benkhalil A. K., Aboudarham J., Fuller N., 2005, *Sol. Phys.*, 228, 399  
 Isobe, H., Tripathi, D., Archontis, V., 2007, *ApJ*, 657, L53  
 Isenberg P. A., Forbes T. G., 2007, *ApJ*, 670, 1453  
 Joshi N.C., Srivastava A.K., Filippov B., Kayshap P., Uddin W., Chandra R., Choudhary D.P., Dwivedi B.N., 2014, *ApJ*, 787, 11  
 Karpen J. T., Antiochos S. K., Klimchuk J. A., MacNeice P. J., 2003, *ApJ*, 593, 1187  
 Kliem B., Török T., 2006, *Phys. Rev. Lett.*, 96(25), 255002  
 Kliem B., Török T., Titov V. S., Lionello R., Linker J. A., Liu R., Liu C., Wang H., 2014, *ApJ*, 792, 107  
 Kumar P., Manoharan P. K., Uddin W., 2010, *ApJ*, 710, 1195  
 Lemen, J. R. et al., 2012, *Sol. Phys.*, 275, 17  
 Leroy, J. L. 1989, in *ASSL 150, Dynamics and Structure of Quiescent Solar Prominences*, p. 77  
 Li L. P., Zhang J., 2013a, *A&A*, 552, L11  
 Li T., Zhang J., 2013b, *ApJ*, 770, L25  
 Li T., Zhang J., 2013c, *ApJ*, 778, L29  
 Lin J., Forbes T.G., Isenberg P.A., Démoulin P., 1998, *ApJ*, 504, 1006  
 Lites B. W., 2005, *ApJ*, 622, 1275  
 Liu R., Liu C., Wang S., Deng N., Wang H., 2010, *ApJ*, 725, L84  
 Liu R., Kliem B., Török T., Liu C., Titov V. S., Lionello R., Linker J. A., Wang H., 2012, *ApJ*, 756, 59  
 Low B. C., 1996, *Sol. Phys.*, 167, 217  
 Mackay D. H., van Ballegooijen A. A., 2005, *ApJ*, 621, L77  
 Mackay D. H., Karpen J. T., Ballester J. L., Schmieder B., Aulanier G., 2010, *Space Sci. Rev.*, 151, 333  
 Martens P. C., Zwaan, C., 2001, *ApJ*, 558, 872  
 Martin S. F., 1998a, *Sol. Phys.*, 182, 107  
 Martin S. F., 1998b, in Webb D., Rust D., Schmieder B., eds, *IAU Colloquium 167, ASP Conference Series 150, New Perspectives on Solar Prominences*, p. 419  
 Martin S. F., Bilimoria R., Tracadas P. W., 1994, in *Solar Surface Magnetism*, Kluwer, Dordrecht, p. 303  
 McIntosh P. S., 1972, *Rev. Geophys. Space Phys.*, 10, 837  
 McKenzie D. E., Canfield R. C., 2008, *A&A*, 481, L65  
 Nindos A., Patsourakos S., Wiegmann T., 2012, *ApJL*, 748, L6  
 Okamoto T. J., Tsuneta S., Lites B. W., et al., 2008, *ApJ*, 673, L215  
 Olmedo O., Zhang J., 2010, *ApJ*, 718, 433  
 Patsourakos S., Vourlidis A., Stenborg G., 2013, *ApJ*, 764, 125  
 Pevtsov A. A., Balasubramaniam K. S., Rogers J. W., 2003, *ApJ*, 595, 500  
 Pneuman G. W., 1983, *Sol. Phys.*, 88, 219  
 Raouafi N.-E., 2009, *ApJ*, 691, L128  
 Rust D. M., 1999, in Brown M. R., Canfield R. C., Pevtsov A. A., eds, *Geophysical Monograph 111, Magnetic Helicity*



- in Space and Laboratory Plasmas, American Geophysical Union, Washington, p. 221
- Rust D. M., Kumar A., 1994, *Sol. Phys.*, 155, 69
- Rust D. M., Martin S. F., 1994, in Balasubramanian K. S., Simon G.W., eds, ASP Conf. Ser. 68, Solar Active Region Evolution: Comparing Models with Observations, p. 337
- Schmieder B., Mein N., Deng Y., Dumitrache C. Malherbe J. M., Staiger J., DeLuca E. E., 2004, *Sol. Phys.*, 223, 119
- Schou J., et al., 2012, *Sol. Phys.*, 275, 229
- Smith S. F., Ramsey H. E., 1967, *Sol. Phys.*, 2, 158
- Snodgrass H. B., Kress J. M., Wilson P. R., 2000, *Sol. Phys.*, 191, 1
- Török T., Chandra R., Pariat E., Démoulin P., Schmieder B., Aulanier G., Linton M. G., Mandrini C. H., 2011, *ApJ*, 728, 65
- van Ballegooijen A. A., Martens, P. C. H., 1989, *ApJ*, 343, 971
- van Tend W., Kuperus M., 1978, *Sol. Phys.*, 59, 115
- Wuelser J.-P. et al., 2004, *Proc. SPIE*, 5171, p. 111
- Zhang M., Low, B. C., 2005, *ARA&A*, 43, 103
- Zhang J., Cheng X., Ding M.-D., 2012, *NatCo*, 3, 747

This paper has been typeset from a  $\mathrm{T}_{\mathrm{E}}\mathrm{X}/\mathrm{L}^{\mathrm{A}}\mathrm{T}_{\mathrm{E}}\mathrm{X}$  file prepared by the author.